Dynamics of the flow inside an urban canopy : Study of the flow in the vicinity of a cube immersed in a thick turbulent boundary layer

Sophie Herpin, Geng Tian, Laurent Perret, Boris Conan, Romain Mathis, Isabelle Calmet

Dynamics of the flow inside an urban canopy : Study of the flow in the vicinity of a cube immersed in a thick turbulent boundary layer

Sophie Herpin[a,b], Geng Tian[a], Laurent Perret[a], Boris Conan[a], Romain Mathis[c] and Isabelle Calmet[a]

a. LHEEA, Ecole Centrale de Nantes, UMR CNRS 6598
b. LML, FRE3723, Ecole Centrale de Lille c. IMFT, UMR 5502 CNRS INPT/UPS France

Résumé :

L'écoulement à l'intérieur d'une canopée urbaine idéalisée constituée d'un quadrillage de cubes arrangés en quinconce et de densité 25%, immergé dans une couche limite atmospherique de Reynolds $Re_\delta = \delta^+ = 32300$ est étudié au moyen de la Velocimétrie Laser Doppler. Le rapport géométrique entre la hauteur de la couche limite et la hauteur de cube $\delta/h = 22.7$, ainsi que le nombre de Reynolds basé sur la hauteur de cube $h^+ = 1420$ sont suffisamment grands pour que les conditions soient représentatives de conditions réelles. La LDV donne accès à des données ponctuelles mais résolues en temps à différentes hauteurs dans la canopée ($z = h/4$, $h/2$, and h) et à différentes positions relativement aux cubes. Ces données sont comparées à des données de Simulation des Grandes Echelles d'une canopée géométriquement similaire à un nombre de Reynolds de $h^+ = 500$ dont les paramètres sont proches de ceux de la DNS de [5]. Les profils verticaux de vitesse moyenne et des tensions de Reynolds sont analysés et comparés à des données de la littérature. L'accord est assez bon, sauf pour la deviation standart de la composante transversale de vitesse qui présente des écarts assez larges. Des cartographies de l'écoulements sont ensuite extraites de la LES et permettent une meilleur compréhension de l'organisation de l'écoulement de canopée. Aux positions où les données de LDV sont disponibles, un bon accord est trouvé. Une analyse spectrale détaillée de la canopée est finalement entreprise. A notre connaissance, c'est la première fois que de tels résultats sur l'évolution de la densité spectrale de puissance à l'intérieur de la canopée sont produits.

Abstract :

The flow inside an idealized urban canopy consisting of an staggered array of cubes with a 25% density, immersed into an atmospheric surface layer with a Reynolds number of $Re_\delta = \delta^+ = 32300$ is investigated by means of Laser Doppler Anemometry. The cube boundary layer thickness to cube height ratio $\delta/h = 22.7$ as well as the Reynods number based on the cube height $h^+ = 1420$ are large enough to be representative of engineering applications. The LDA data gives access to pointwise time-resolved data at several positions inside the canopy ($z = h/4$, $h/2$, and h) and is compared with LES data of a similar canopy, at $h^+ = 500$ with parameters close the DNS data from [5]. The wall-normal mean velocity profile and Reynolds stresses of both the LDA and LES data show a good agreement with available data in the literature, although some differences are observed on the standard deviation of the spanwise component. Maps of the flow in wall-normal planes inside the canopy extracted from the LES data are

analyzed and allow a better understanding of organization of the canopy flow. Values at the positions of the LDA measurements points are extracted from the LES data and show a reasonnable agreement. A detailed spectral analysis is then carried out using the LDA data. To our knwowledge, this is the first time such results are shown on the evolution of the power spectral density inside the canopy.

Mots clefs : Turbulence, couche limite atmosphérique, Canopée urbaine, Vélocimétrie Laser Doppler, Simulation des Grandes Echelles

1 State of the Art

Understanding atmospheric flows in urban areas is of primary importance in the context of urban densification of the worldwide population. While the flow inside an urban-type roughness has been described statistically [7], its dynamics has never been fully addressed. From a purely aerodynamic point of view, the flow inside an urban canopy can be seen as the flow developing around three-dimensional obstacles (induced by the buildings geometry) immersed into a high Reynolds number, rough boundary layer flow (the atmospheric surface layer), with complex interactions [1].

Despite the very large range of building size, shape, or spatial arrangement in real-life built areas, the simplified canopy consisting of a regular array of cubes is now widely accepted as a canonical representation. Several contributions investigating the turbulent flow around a single wall-mounted cube can be found in the literature ([8] ; [14]) and are a good starting point to understand the dynamics inside such a canopy. Using flow visualizations, [8] proposed a very comprehensive representation of the flow around a single mounted cube (figure 1). On the upstream face of the cube, the incoming flow is deviated by the presence of the cube, with a spanwise by-pass motion of the sides of the cube and a vertical by-pass motion on the top of the cube. The sharp edges of the cube induce a flow separation on the sides and top of the cube, with a vertical and spanwise vortex shedding respectively. Close to the wall, in the upstream stagnation region of the cube, a large horseshoe vortex is formed, with a spanwise head attached in the upstream region of the cube and two long streamwise legs extending downstream on each side of the cube. An elongated recirculation region is visible in the downstream region of the cube, with a second attached horshoe vortex attached to the cube. Further downstream, the wake of the cube is characterized by increased turbulence and lower mean streamwise velocity.
However, the flowfield becomes more complex over an array of cubes. [10] and [6] identified three flow regimes, the isolated roughness flow, the wake interference flow, and the skimming flow, depending on the packing area density of the urban roughness (see figure 2).

[9] proposed a very interesting wind-tunnel study of a regular array of large cubes cube ($H/h = 3.4$, with H the wind-tunnel height), at a Reynolds number $Re_h = 3854$ (based on the cube height and the bulk velocity). The cubes were all aligned in both the streamwise and spanwise direction (square pattern), thus making room for spanwise and streamwise alleys with full clearance between the cubes ; the cube array density was 6.25%. The authors used flow visualisations and Laser Doppler measurements to investigate the organisation and the dynamics of the flow. The organisation of the flow was found to be quite coherent with earlier studies on single-cube flow, and a vortex shedding could be identified on the sides of the cube using the power spectral density of the spanwise velocity component, with a Strouhal number about 0.1, based on the cube height and the bulk velocity. The good agreement with single cube flow was expected since the fairly low cube density corresponds to the "isolated roughness flow regime".

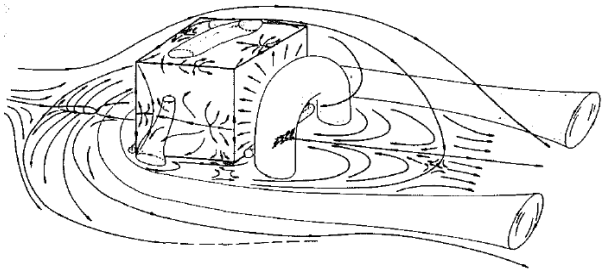

Figure 1: Schematic representation of the flow around a single mounted cube, from [8]

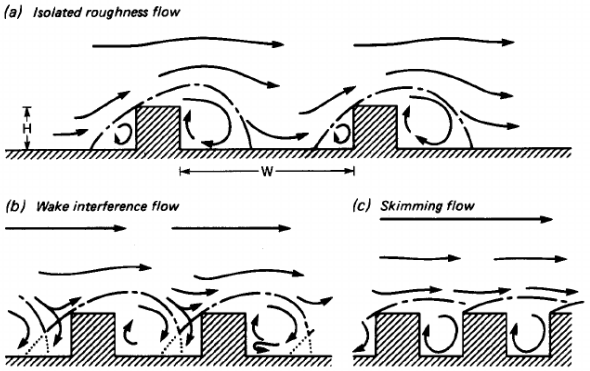

Figure 2: The three flow regimes in an array of cubes from [10]

Later studies investigated the turbulent flow developping over more dense arrays of cubes (25% density), pertaining to the wake interference flow regime.

Due to the tight clearance and high complexity of the flow, wind-tunnel measurements within a dense canopy are not straightforward, and relatively little time-resolved experimental data can be found. In that perspective, the work from Castro's group ([2]) using Laser Doppler Anemometry (LDA) is a major step forward to study the flow dynamics in this region. The mean velocity and turbulent stresses wall-normal profiles were obtained within a staggered 25% canopy and above the roughness, at four positions P1, P2, P3, P4 representatives of the cube array pattern, in a conventionnal wind-tunnel with a ratio $\delta/h = 7.4$ and at moderate Reynolds number. The mean velocity profile was found to exhibit significant differences inside the urban canopy, especially at points P1 (downstream of the cube) and P2 (upstream of a cube) where an inflexion point was found at about $h/2$. On the Reynolds stresses, a maximum was found near the canopy roof, especially at point P1 in connection with the shear layer separating from the top leading edge of the cube. Two-points correlations and power spectral density analysis were carried out but restricted to the roughness sublayer and therefore time scales, length scales, or structure angles were not given inside the canopy.

On the numerical side, [5] performed an obstacle-resolving DNS of a turbulent boundary layer over 25% canopies (with staggered, aligned, and square spatial arrangment), and carried out an analysis of the mean velocity and the turbulent stresses; a good agreement was found with the experimental data of [3] and [2] ; it was also found that, for a given density, these statistics depend significantly on the cube pattern. In a subsequent study on their DNS data with the staggered 25% canopy, [4] investigated the coherent structures inside the logarithmic region above the roughness, using two-points correlations, quadrant analysis, and visualisations of iso-surfaces with a suitable vortex detection variable.

Two main limitations arise from the above-mentionned studies : the datasets are obtained at moderate Reynolds number (typically $Re_\tau = h^+ = 500$) as well as with small boundary layer thickness (δ) to cube height (h) ratio (typically 8 [4]), due to CPU limitations on DNS ([5],[4]) or to the limited thickness of the boundary layer in conventionnal wind-tunnels([3],[2]). This does not enables a faithful reproduction of the very large scale motions in the outer region of real atmospheric flows, and therefore of the complex inner/outer interactions with the canopy flow.

In the present contribution, we focus our attention on the dynamics of the flow within a 25% density array of staggered cubes immersed into a turbulent boundary layer flow. Two datasets are used : an LES dataset with main parameters close to the sudy of [4], giving full access to spatial content of the flow, as well as a time-resolved LDA dataset obtained in an atmospheric wind-tunnel at high Reynolds number

($h+ = 1420$ and $\delta^+ = 32300$), and with a ratio $\delta/h = 22.7$ significantly larger than previous studies in the litterature, and more representative of engineering applications. The statistical picture of the flow within the canopy is first analyzed and assessed against existing data in the literature. Taking advantage of the good temporal resolution of both experimental and numerical data, we then focus our analysis on the dynamics of the flow in the vicinity of a cube. A detailed temporal spectral analysis is carried out on the LDA and LES data to extract quantitative information; in particular, it is checked whether the vortex shedding typically observed on the sides of an isolated cube is still present inside a canopy in the wake interference regime.

2 Experimental and Numerical Design

2.1 Experimental Design

The flow under investigation is simulated inside the LHEEA atmospheric wind-tunnel at Ecole Centrale de Nantes ([12]). After appropriate conditionning with spires and fence, the atmospheric surface layer develops over a 24m long floor, fully covered with an urban canopy consisting of a regular, staggered array of $h = 50$ mm-high cubes with a packing area density of 25%. The main characteristics of the flow are summarized in table 1. More details on the turbulent boundary layer flow, as well as on the estimation of the friction velocity, displacement thickness and aerodynamic roughness length can be found in [11].

U_e	δ	u_*	δ/h	$u_\star/Ue$	$Re_\delta = \delta^+$	$Re_h = h^+$	z_0/h	d/h
5.78 m/s	1.134m	0.4278 m/s	22.7	0.074	32300	1420	0.11	0.59

Table 1: Main characteristics of the flow ; z_0 is the aerodynamic roughness length and $d = \delta^*$ the displacement thickness

The dynamics of the flow inside the canopy was recorded using a 2 Components Laser Doppler Anemometry System from Dantec Dynamics (model FlowExplorer DPSS), operating in backward scattering mode. The LDA probe is equipped with a 300 mm focal length, and the measurement volume is illuminated using two lasers emitting at 532 nm and 561 nm with a maximum power of 300 mW. A schematic representation of the experimental setup is shown in figure 3. In this study, the streamwise, spanwise and wall-normal directions are denoted x, y, z respectively and associated with velocity components u, v, w. The probe is positioned below the wind-tunnel floor and oriented vertically ; the floor of the wind-tunnel is equipped with a transparent window to ensure optical access to the flow inside the canopy. This configuration enables the measurement of the streamwise u and spanwise v velocity components inside the canopy. The measurement volume size is $\Delta x = \Delta y = 0.1$ mm and $\Delta z = 1$ mm, or in wall units $\Delta x^+ = \Delta y^+ = 2$ and $\Delta z^+ = 20$.

Sixteen positions were recorded within the canopy (figure 4), distributed at three altitudes with respect to the cube height : $z = 0.25h$, $0.5h$ and $1h$, and at longitudinal/spanwise positions representative of the canopy pattern (P1, P2, P3 as defined by Castro) as well as additional points (A, B, C, D) chosen to study the flow dynamics in the vicinity of a cube. One additionnal point, E, located 1h downstream of the trailing edge of a cube, was also measured using LDA at three heights above the canopy ($z = 1.25h$, $1.45h$ and $5h$). This point was used to validate the LDA data against available data measured using how-wire anemometry and also to compare the dynamics of the flow in the canopy with the dynamics in roughness and inertial region.

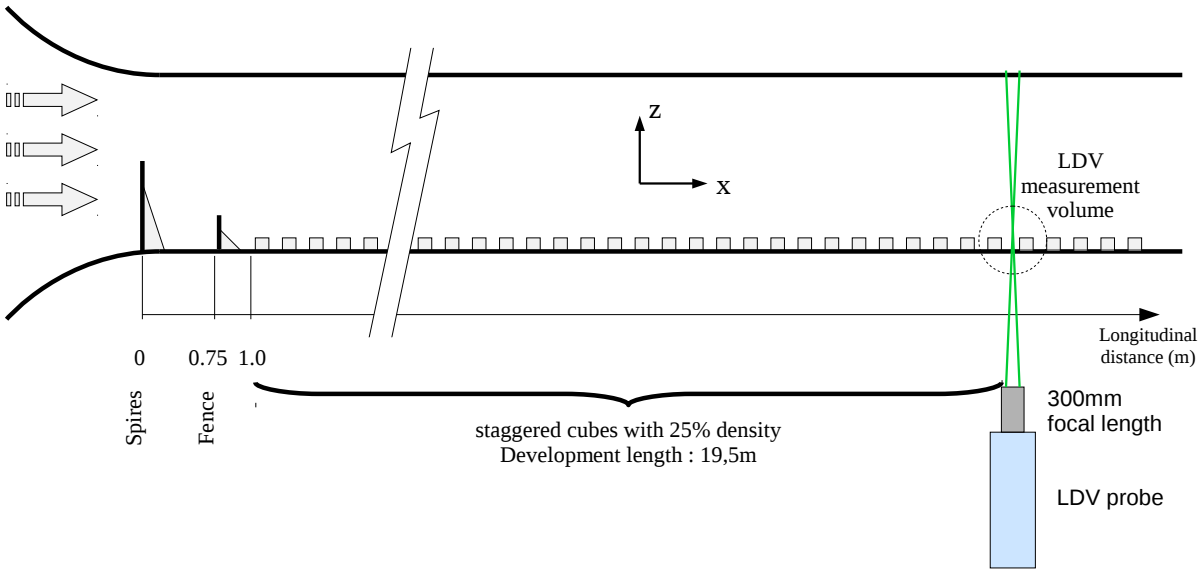

Figure 3: Schematic representation of LDV measurement setup

The mean LDA datarate was varying with the position of the measurement point. The raw mean

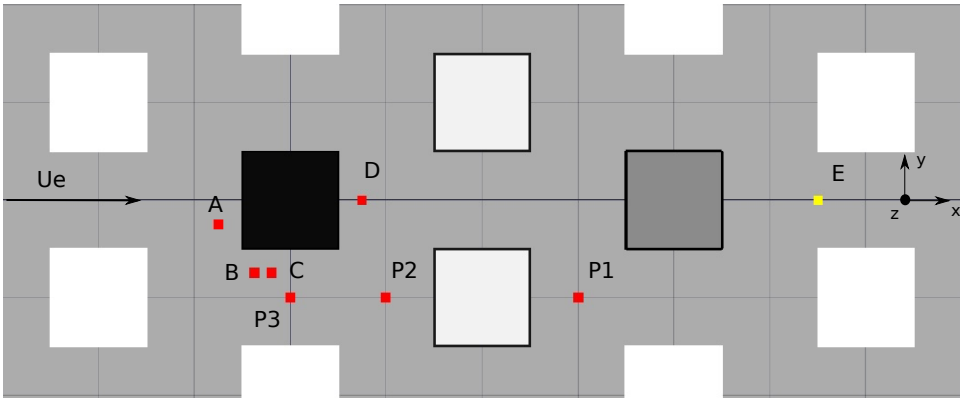

Figure 4: Positions of the LDA measurement points in a wall-parallel (XY) plane

datarate increased with the distance to the wall and typically varied between 150 Hz and 1300 Hz inside the canopy and up to 1617 Hz above the canopy. After acquisition, inter-arrival time of particles were computed on the raw data inside the canopy, and measurement points with an inter-arrival time lower 0.25 ms (corresponding to an instantaneous datarate higher than 4000 Hz) were removed from the dataset. This cut-off frequency was chosen after careful inspection of the PDF of the inter-arrival times. It is approximately the cut-off frequency given by the LDA measurement volume size and the friction velocity $f_{\text{cut-off}} = u_*/\Delta x = 4277$ Hz, meaning that all particles with a lower inter-arrival time (or conversely a higher datarate) have overlapping residence time inside the LDA measurement volume, or are counted twice and may therefore lead to an incorrect evaluation of the doppler burst.

A subsequent outliers detection was performed on both velocity components and points such that $|(u_i - \bar{u_i})| > \sigma * (5 + \text{skewness})$ were removed. The skewness of the velocity distribution was included to take into account non-normal PDF distribution in the canopy (typically observed on the streamwise velocity at the canopy interface ($z = h$)). In any case the percentage of outliers detected was very low, under 0.1%. The final effective mean datarate obtained for each measurement point is finally shown in table

2, the lowest datarate being 99 Hz and the largest 836 Hz. The duration of the LDA acquisition is also reported in table 2 : the LDA signal was acquired over 1200 seconds (20 minutes) for each point at z=h/4 and over 3600 seconds (1 hour) for each point at $z = h/2$, h, $1.25h$, $1.45h$, $5h$.
These datarates and acquisition times should be compared with the main frequencies (and the inverse quantity, the turn-over time) in the flow that can be estimated using the flow main parameters : U_e and δ for the outer flow and u_* and h for the flow inside the canopy. The results are shown in table (3). The LDA datarates are thus between 1 and 2 order of magnitude higher than the expected characteristics frequencies of the flow, which ensures an appropriate time resolution of the flow dynamics. The acquisition time at $z = h/4$ corresponds to 10000 turn-over times in inner scaling and to 6000 turn-over times in outer scaling ; the acquisition time at $z = h/2$ and $z = h$ corresponds to 30000 turn-over times in outer scaling and to 18000 turn-over times in inner scaling. These very long acquisition times were chosen to reach good statistical convergence of high-order quantities. Both datarate and sampling time allow us to converge small to large scale content.

LDA point	z/h	Mean Datarate (Hz)		Acquisition time (s)
B	1/4	168		
P2	1/4	115	137	1200
P3	1/4	129		
A	1/2	144		
B	1/2	99		
C	1/2	148	175	3600
P1	1/2	337		
P2	1/2	232		
P3	1/2	223		
A	1	836		
B	1	588		
C	1	232		
D	1	121	453	3600
P1	1	471		
P2	1	431		
P3	1	491		

Table 2: Mean Effective datarate for each LDA point

$f_{\text{outer, LDA}}$ (Hz)	$f_{\text{inner,LDA}}$ (Hz)	$t_{\text{outer,LDA}}$ (s)	$t_{\text{inner, LDA}}$ (s)
5.1	8.6	0.2	0.12

Table 3: Characteristic Frequencies and turn-over times in the wind-tunnel flow in the outer and inner region

2.2 Numerical Design

The filtered Navier-Stokes equations are written as follow:

$$\frac{\partial u_i}{\partial x_i} = 0 \tag{1}$$

$$\frac{\partial u_i}{\partial t} + \frac{\partial u_i u_j}{\partial x_j} = -\frac{1}{\rho}\frac{\partial p}{\partial x_i} + \nu\frac{\partial^2 u_i^2}{\partial x_j} - \frac{\partial \tau_{ij}}{\partial x_j} - f_i \tag{2}$$

In equations (1) and (2) the variables $\boldsymbol{u_i}$ and $\boldsymbol{p}$ represent the resolved-scale (filtered) velocity and pressure respectively, $\boldsymbol{\nu}$ is the fluid kinematic viscosity. The SGS stress tensor τ_{ij} is modeled following Smagorinsky [13] :

$$\tau_{ij} = -2\nu_{sgs}S_{ij} \tag{3}$$

where the resolved stain rate tensor is defined as:

$$S_{ij} = \frac{1}{2}\left(\frac{\partial u_i}{\partial x_j} + \frac{\partial u_j}{\partial x_i}\right) \tag{4}$$

and the SGS kinetic viscosity ν_{sgs} is modelled as:

$$\nu_{sgs} = {C_S}^2 \Delta^2 \sqrt{2S_{ij}S_{ij}} \tag{5}$$

The drag force f_i introduced in (2) to model the influence of the canopy in the drag-porosity approach is defined by:

$$f_i = \frac{1}{2}C_D(z)\alpha u_i\sqrt{u_k u_k} \tag{6}$$

where $C_D(z)$ is the drag coefficient profile extracted from obstacle-resolved simulation and α is the volumetric frontal density. In our configuration, $\alpha = 1/3h$, where h is the obstacle height. Note that $f_i = 0$ in the obstacle-resolved simulations.

The code is developed on the open source software $OpenFOAM2.4.0$, which uses finite volume method, combined with LES and standard Smagorinsky SGS model (equations (3)-(5)) with $C_S = 0.167$. Equations are solved using second-order implicit linear differencing for the spatial derivatives and second-order implicit linear backward differencing for the temporal integration. Figure 5 shows a plan view of the computational domain, with staggered cube arrays of dimensions $16h \times 12h \times 8h$. The finest grid used is $h/32$. Coceal [5] have confirmed that the simulations over cubic geometry are generally well resolved by $h/32$ mesh. Free-slip boundary condition is applied at the top of the domain. No-slip condition applied at the bottom and on all obstacle surfaces. Periodic boundary conditions are imposed both in span-wise and stream-wise directions to simulate an infinite array. The Reynolds number of the flow, based on the velocity at the top of the domain and the obstacle height is about 5000. The roughness Reynolds number R_τ based on the friction velocity u_* and obstacle height is about 500. To ensure the flow temporal convergence, simulations were run for an initial duration about $250T$, where $T = h/u_*$ is an eddy turnover time for the largest eddies shed by the cubes [5] . Statistics were collected and averaged over a further duration of $220T$ for computing flow statistics and turbulent kinetic energy budget.

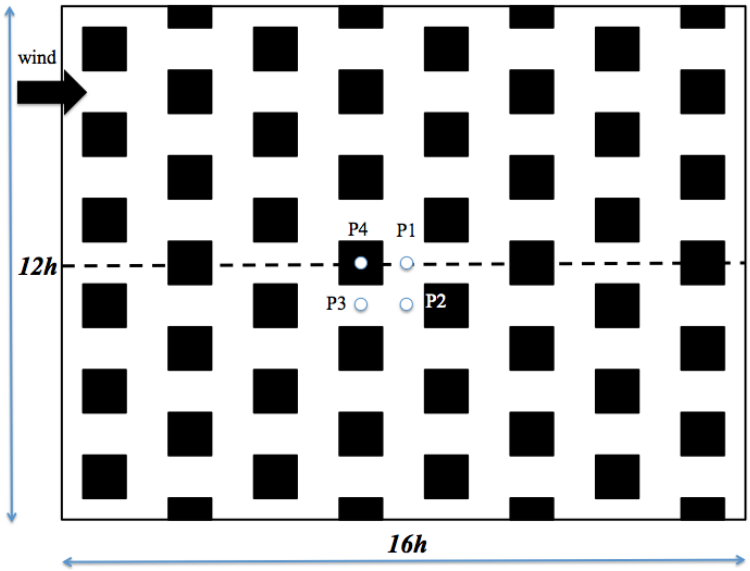

Figure 5: Plan view of the computational domain of the obstacle-resolved simulation

The flow bulk velocity (that will be used as the characteristic velocity for the outer flow) is $U_b = 2.6$ m/s. As we did for the LDA data, we can also compute characteristics frequency and timescale of the flow using inner and outer scaling. The results are shown in table 4.

$f_{\text{outer,LES}}$ (Hz)	$f_{\text{inner,LES}}$ (Hz)	$t_{\text{outer, LES}}$ (s)	$t_{\text{inner, LES}}$ (s)
16.25	14.25	0.06	0.07

Table 4: Characteristic Frequencies and turn-over times in the LES in the outer and inner region

3 Statistical Description of the Flow field inside the canopy

3.1 Vertical Profiles of Mean Velocity and Standard deviations

The mean profiles of U, u_{RMS} and v_{RMS} at points P1, P2, P3, in inner scaling (i.e u_* for the velocity and h for the altitude z) for the LDA and LES datasets are shown in figure 6, and compared with the LDA data of [2] and the DNS data of [4].

3.1.1 A note about the averaging scheme of the LDA data

The LDA statistics were computed using 2 averaging schemes: a regular arithmetic average, and a Transit-Time weighting average. Overall, the magnitude of the weighted LDA statistics is always lower than the regular arithmetic average, as expected because the transit-time weighting is meant to compensate for a bias of the LDA technique towards high-velocities. In all statistics that will be analyzed in details below, the magnitude of the LDA data from Castro group ([2]) is always found to be higher than the other datasets, including our LES, the DNS from [4] and our LDA data. This little over-estimation of the LDA data from Castro was already spotted by [4]. We found no details on the averaging procedure

or weighting scheme employed by Castro-group to compute statistics on the LDA data, but overall their data are closer to our LDA results when no weighting scheme is employed.

3.1.2 Mean Velocity profile

Overall, the mean streamwise velocity profile show a good collapse of all the data, which confirm that the inner scaling is appropriate for the mean flow inside the canopy.
The point P1, located at 0.5h downstream of the leeward face of a cube, is located inside a sheltered area, and the mean streamwise velocity is close to 0 for $0.3 \leq z/h \leq 0.8$. In the immediate vicinity of the wall ($z/h \leq 0.3$), a recirculation region is visible. This recirculation area is best described by the LES and DNS where data is obtained down to the wall, while the experimental data (present data as well as Castro'group data [2]) lowest position is located at $z/h = 0.25$ and only gives information on the top part of this recirculation region. Close to the canopy roof ($z/h \geq 0.8$)) a steep velocity gradient, almost constant up to $z/h \leq 1.1$, can be observed, indicating the presence of a shear layer between the outer and the inner flow in this region. The collapse between all data at P1 is very good, except at $z = h$ where some differences can be observed, but this position is right inside the strong velocity gradient region, so differences can be explained by a slight shift in the z measuring position.
At point P2, $0.5h$ upstream of the windward face of a cube, a recirculation region is also visible through negative velocity for $z \leq 0.2$, and the profile shows two inflexion points, the first one at $z/h = 0.4$ at the interface between the top of a vortical structure (which corresponds to the spanwise head of the horshoe vortex observed in single cube) and the flow in the upper half of the canopy, and the second inflexion point is located at $z/h = 0.1$ which corresponds to the interface between the bottom of this horshoe vortex and the no-slip layer next to the wall. This wall-normal profile is in full agreement with the streamwise/wall-normal mean velocity field extracted through the middle of a cube by [5]. Above $z = h/4$ the mean velocity increases regularly, and up to the canopy roof.
At point P3, in the middle of a streamwise alley, it is worth noting that the LDA mean velocity data is about 10-20% lower than the other data. Aside this shift, the trend for all dataset is similar. Close to the wall, below $z = 0.1h$ a local peak of velocity can be found. Above this, the velocity profile display a regular increase throughout the cube height.
Finally, although the flow is quite heterogeneous inside the canopy, the profiles of P1, P2, and P3 seem merge to similar values from $z/h \geq 1.1$.

3.1.3 Standard deviation of U

The profile of the standard deviation of U is also shown in figure 6. Again a good collapse of the data is obtained, indicating that u_* and h are appropriate scaling for the fluctuating streamwise velocity.
A point P1 (downstream of a cube) the standard deviation profile is similar to the mean velocity profile with an almost constant u_{RMS} for $z/h < 0.8$, with $u_{RMS}/u_* \approx 0.6$ and then a sharp increase for $0.8 \leq z/h \leq 1.1$, in connection with the shear layer developping from the trailing edge of the cube. A peak of turbulence is clearly visible at $z/h = 1.1$.
At point P2 (upstream of a cube), the collapse of all data is very good. A minimum of u_{RMS} is obtained at $z/h = 0.25$, indicating that the recirculation region identified on the mean profile, possibly linked to the presence of the head of a horshoe vortex, is quite stable and is not associated with a high level of turbulence. For $z/h \geq 0.25$ the profile increases regularly from a value of $< u > /u_* = 1$ to a value of

$< u > /u_* = 1.7$ at the canopy roof.
At point P3, a good collapse of the data is obtained between LES and weighted LDA. The standard deviation is quite constant close to the wall, for $z/h < 0.25$ and then shows a regular increase for $0.25 \leq z/h \leq 0.8$. The increase in turbulence becomes more sharp for $z/h \geq 0.8$ possibly due to the interaction with the outer flow.

3.1.4 Standard deviation of V

The profile of the standard deviation of the spanwise velocity v_{RMS} is shown in figure 6. No data from [4] was available on this quantity. The collapse in inner scaling is not as good as for the previous quantities, and significant scatter of the data is visible.
At point P1, the LES data show a trend which is similar to the Castro group data (with a rather flat v_{RMS} for $z/h \geq 0.2$), but the magnitude of our LES data ($v_{RMS}/u_* \approx 0.7$) is two times lower than Castro's data ($v_{RMS}/u_* \approx 1.45$). At $z/h = 0.5$, our LDA data is in very good agreement with Castro data, but at $z/h = 1$, the LDA data falls in between the LES and Castro' data.
At point P2, v_{RMS} increases regularly from the wall up to the canopy roof with a logarithmic trend on the LES data, and a more linear trend on the LDA data from [2].
The profile for v_{RMS} at P3 is quite similar to the profile at P2. Our LDA point at $z = h/2$ is clearly an outlier, possibly due to a measurement issue on the V component at this point and height.
At the canopy roof, all dataset show a rather homogeneous behavior among the points P1, P2, P3.

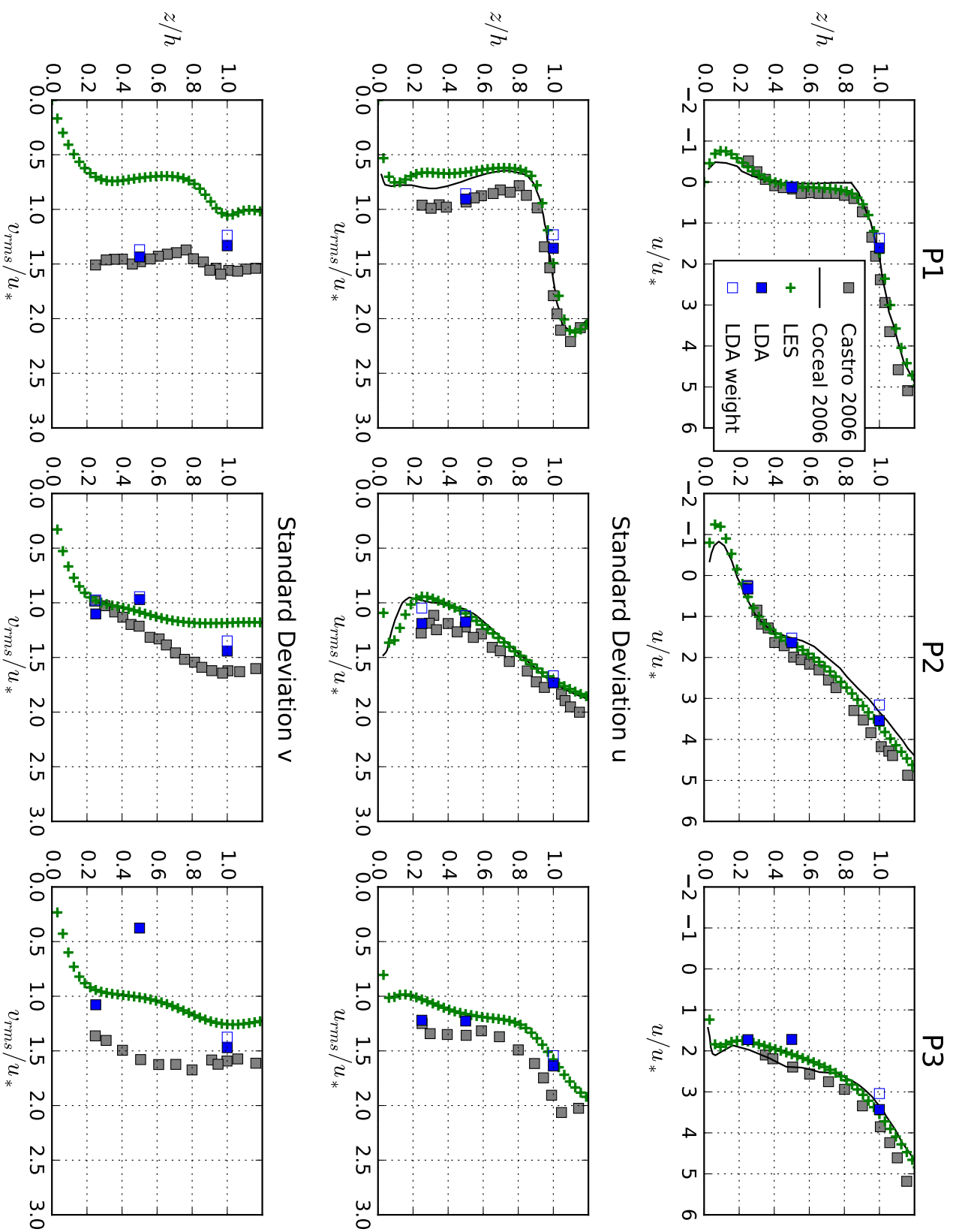

Figure 6: Vertical Profiles of Mean Streamwise Velocity (top) and Standard deviation of streamwise velocity (middle), Standard deviation of spanwise velocity (bottom) at P1 (left), P2 (middle), P3 (right) in LDA and LES data, compared with [2] and [4]

3.2 Flow field in wall-parallel planes

In order to get a comprehensive view of the spatial organization of the flow at all points in wall-parallel planes, maps of mean streamwise velocity (figure 7), mean spanwise velocity (figure 8), standard deviation of streamwise (figure 9) and spanwise (figure 10) velocity, and covariance of u and v (figure 11) at the three heights in the canopy are provided.

On each figure the LDA data are shown on the left hand side, and the LES data are shown on the right hand side. To facilitate the qualitative comparison between LDA and LES data, the same colormap is used and the position of the LDA measurements are reported in the LES map using a black circle. The numerical values obtained at the LDA points in each dataset is also reported for a more quantitative comparison. All data are scaled using u_* and indeed all the values we get are of this order indicating that it is an appropriate scaling for the mean and fluctuating flow inside the canopy.
It should be noted that to get a more comprehensive view of the LDA maps, the LDA results have been periodized through the pattern shown in these figures. Also, the LES data is taken only over one pattern chosen in the middle of the canopy floor, which may explain that the LES data shown in these figures is not always fully converged and therefore fully symetric.
From a qualitative point of view, the mean streamwise velocity maps (figure 7) of the two datasets are quite similar. At the canopy roof, the flow is rather uniform except for the sheltered region with low velocity downstream of the cube (D and P1). The streamwise velocity magnitude of the LES is systematically $15\% - 20\%$ higher than in the LDA data ; this region has a strong velocity gradient, so the difference may be attributed to a small shift in the altitude of the measured points of the LDA. No recirculation region, neither in the downstream part or on the sides of the cube, is visible. The planes at $z = h/2$ and $z = h/4$ show a more heterogeneous flow. An acceleration of the flow at the corner of the cube (B) and on the centerline in between two cubes (P3) is visible, as well as a larger sheltered region downstream of the cube (P1) ; the LES data show a recirculation region with negative velocity immediately downstream of the cube (dashed line in figure 7) ; the extent of this region is larger for $z = h/4$. Upstream of a cube, the deceleration of the flow is visible, this region being of larger extent at $z = h/4$ than at $z = h/2$ (P1 being part of it for $z = h/4$, but not for $z = h/2$), and accordingly the gradient is steeper at $z = h/2$. From a quantitative point of view, the values are in good agreement at $z = h/2$, and slightly higher on the LES data than in the LDA data at $z = h/4$.

In the map of the mean spanwise velocity (figure 8), the spanwise velocity is zero at points P1, P2, P3 on both the LES and LDA data, as expected due to the symmetry of the flow. These zero values are not reported on the figure. The by-pass motion on each side of the cube is clearly visible, and is the strongest at $z = h/2$. The LDA and LES are in very good agreement at $z = h$ and $h/2$, with a slight difference at point B for $z = h/4$.

The standard deviation of u (figure 9) increases slowly with wall normal distance and is quite homogeneous inside each wall-parallel plane. The LDA and LES are in excellent agreement, except for point B at $z = h/2$ and $h/4$ where the LDA standard deviation of the velocity is found to be stronger than the LES one.
The standard deviation of v (figure 10) is quite homogeneous at $z = h$, but shows some spatial variations at $z = h/2$ and $z = h/4$. The activity seems to be concentrated on the sides of the cubes (B), at P3, and at P1. On the LDA data, the value at point P3 at $z = h/2$ is clearly underestimated, as already stated

in the analysis of the vertical profiles. This datapoint will be disregarded for the spectral analysis on the spanwise velocity.

The covariance $< uv >$ (figure 11) has zero values as expected at points P1, P2, P3 on both LES and LDA data (the zeros values are omitted on the figure). On the canopy roof, the covariance is very weak throughout the XY plane. The main activity is obtained at $z = h/2$ and $z = h/4$, at point B, possibly associated to a vertical vortex shedding from the side edges of the cube.

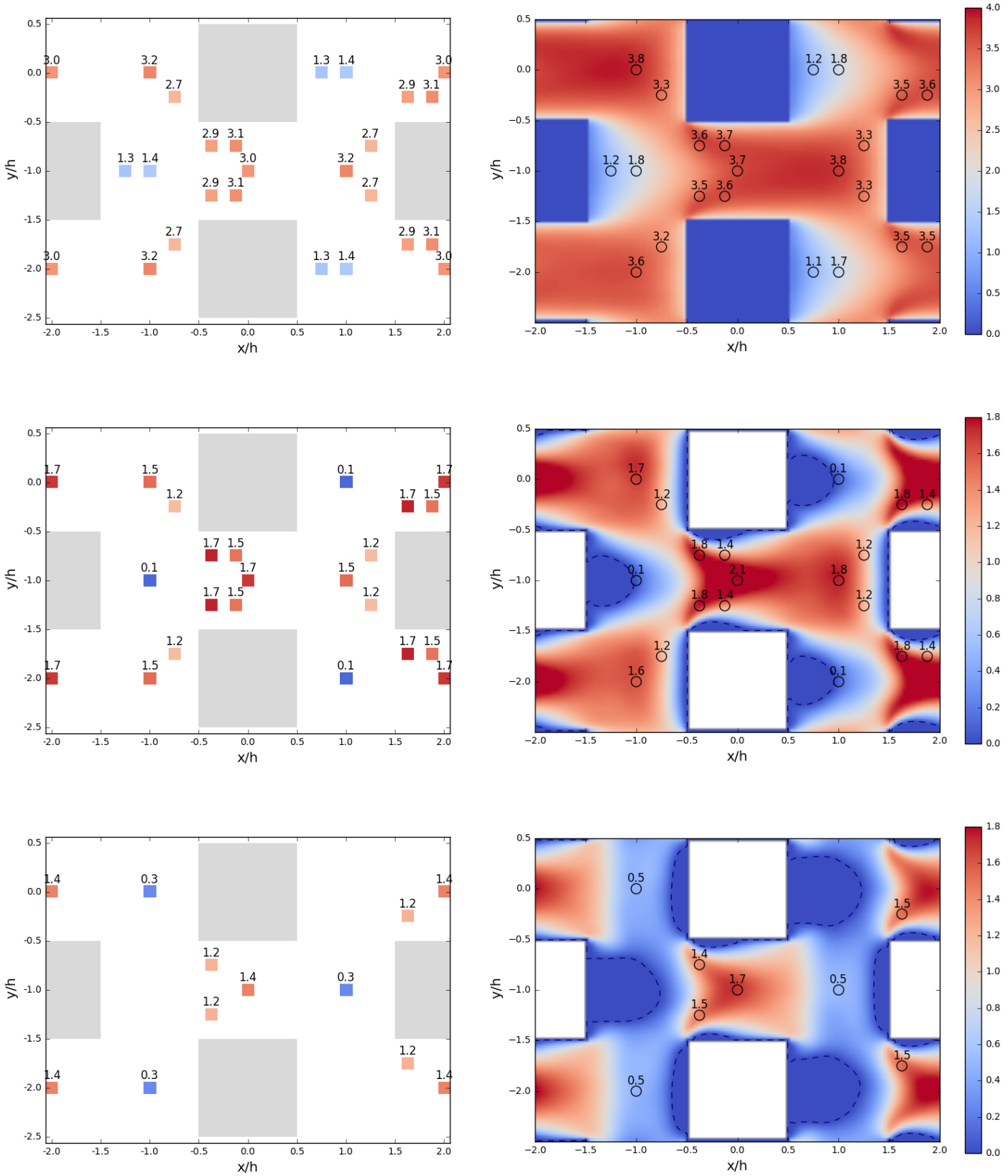

Figure 7: Maps of **mean streamwise velocity** $< u > /u_*$ in wall-parallel planes inside the canopy at various heights : $z = h$ (top), $z = h/2$ (middle), $z = h/4$ (bottom), obtained with LDA data (left) and LES data (right). On the LES maps, the position of the LDA points have been reported with black circles ; the dashed lines corresponds the 0 velocity contour. On both maps, numerical values of mean streamwise velocity $< u > /u_*$ obtained at the positions of LDA points have been reported. The same colormap is used.

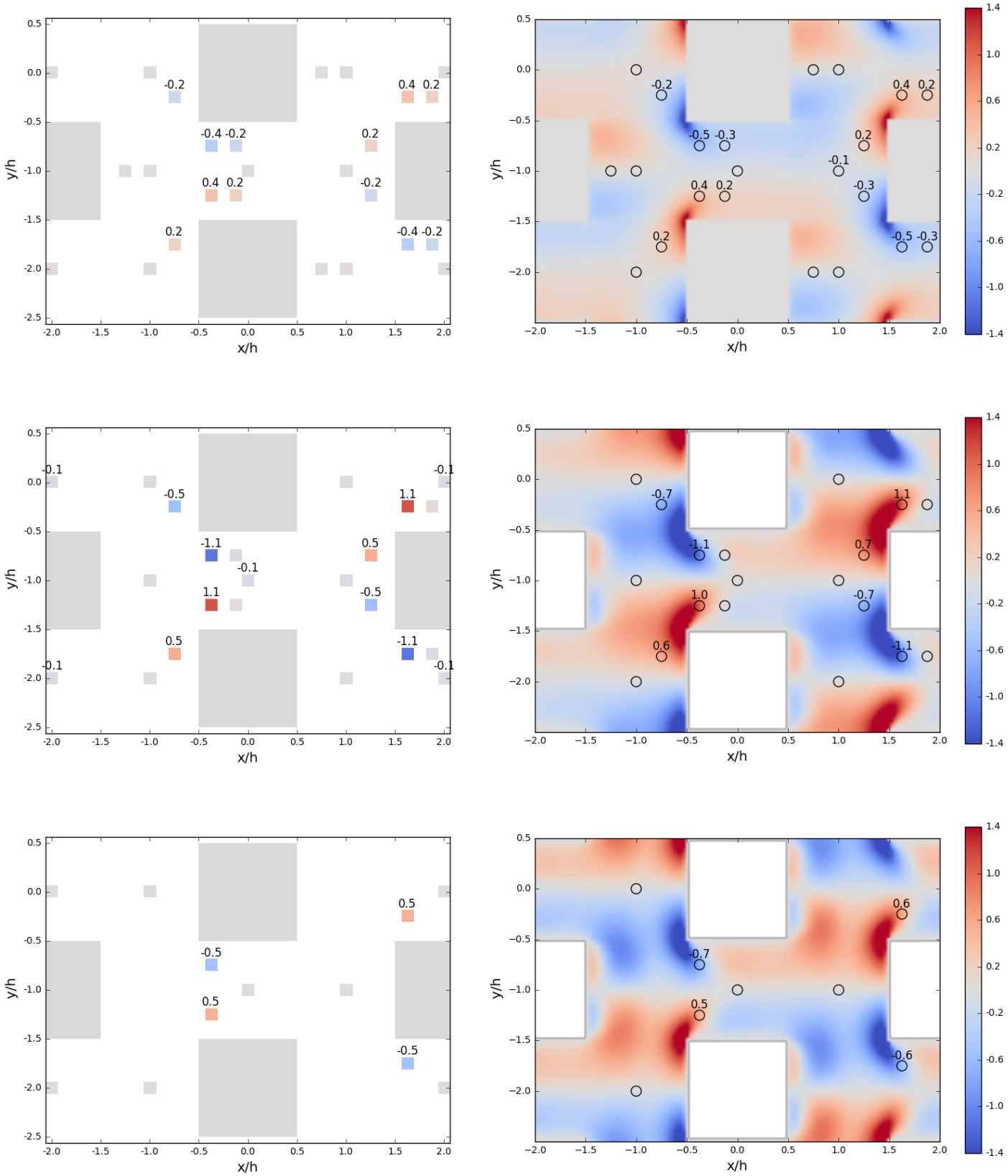

Figure 8: Maps of **mean spanwise velocity** $< v > /u_*$ in wall-parallel planes inside the canopy at various heights : $z = h$ (top), $z = h/2$ (middle), $z = h/4$ (bottom), obtained with LDA data (left) and LES data (right). On the LES maps, the position of the LDA points have been reported with black circles. On both maps, numerical values of mean spanwise velocity $< v > /u_*$ obtained at the positions of LDA points have been reported. The same colormap is used.

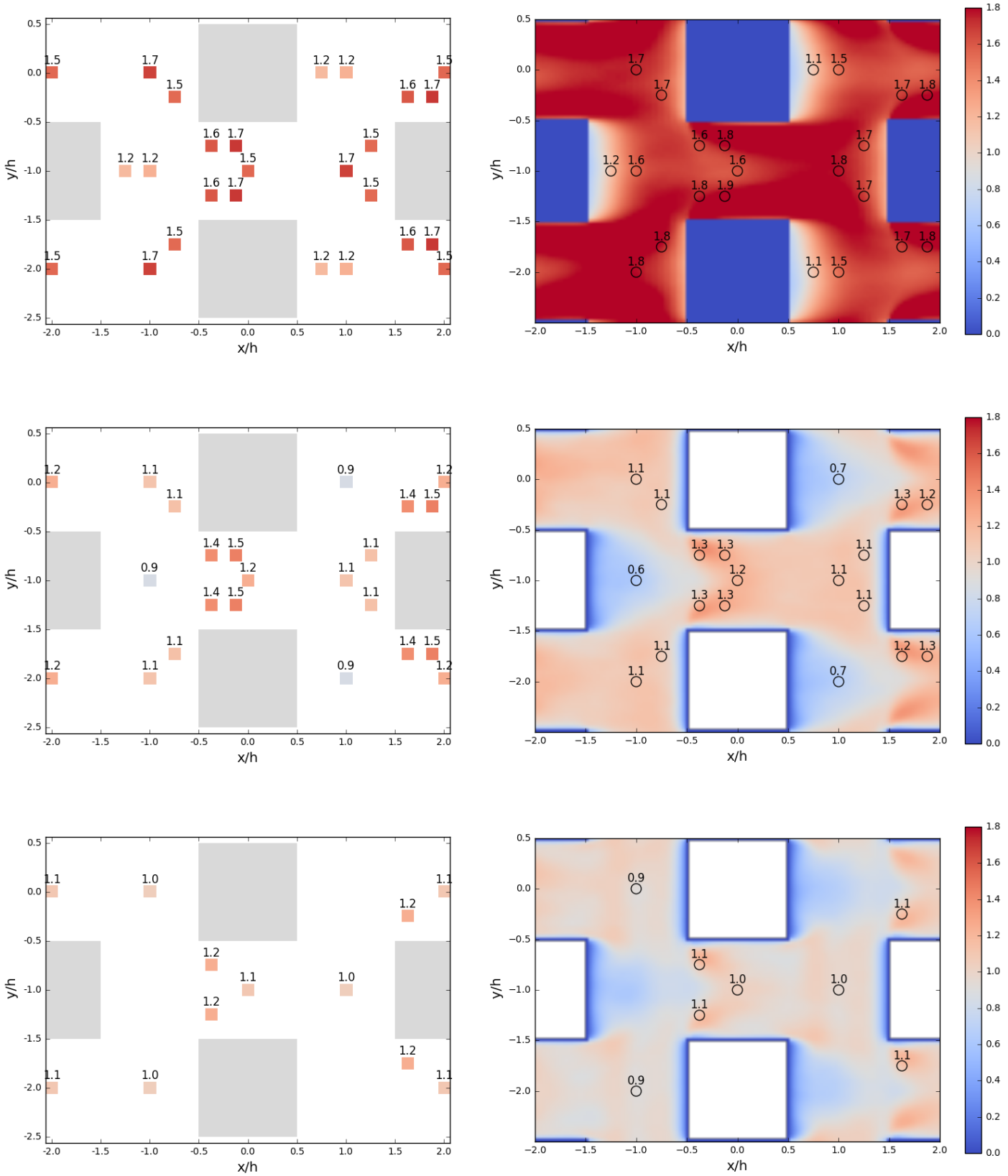

Figure 9: Maps of **Standard deviation of streamwise velocity** u_{RMS}/u_* in wall-parallel planes inside the canopy at various heights : $z = h$ (top), $z = h/2$ (middle), $z = h/4$ (bottom), obtained with LDA data (left) and LES data (right). On the LES maps, the position of the LDA points have been reported with black circles. On both maps, numerical values of Standard deviation of streamwise velocity u_{RMS}/u_* obtained at the positions of LDA points have been reported. The same colormap is used.

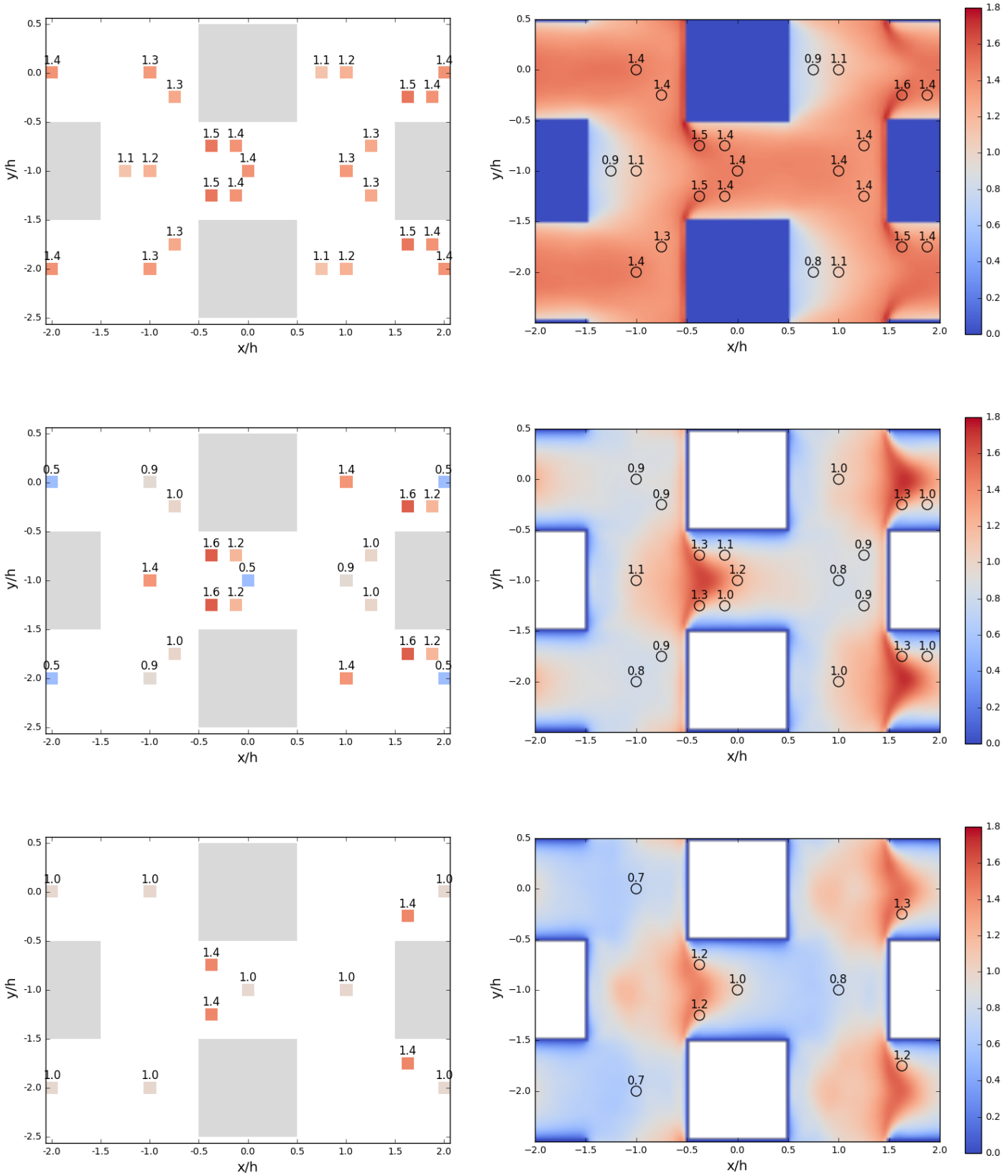

Figure 10: Maps of **Standard deviation of spanwise velocity** v_{RMS}/u_* in wall-parallel planes inside the canopy at various heights : $z = h$ (top), $z = h/2$ (middle), $z = h/4$ (bottom), obtained with LDA data (left) and LES data (right). On the LES maps, the position of the LDA points have been reported with black circles. On both maps, numerical values of Standard deviation of spanwise velocity u_{RMS}/u_* obtained at the positions of LDA points have been reported. The same colormap is used.

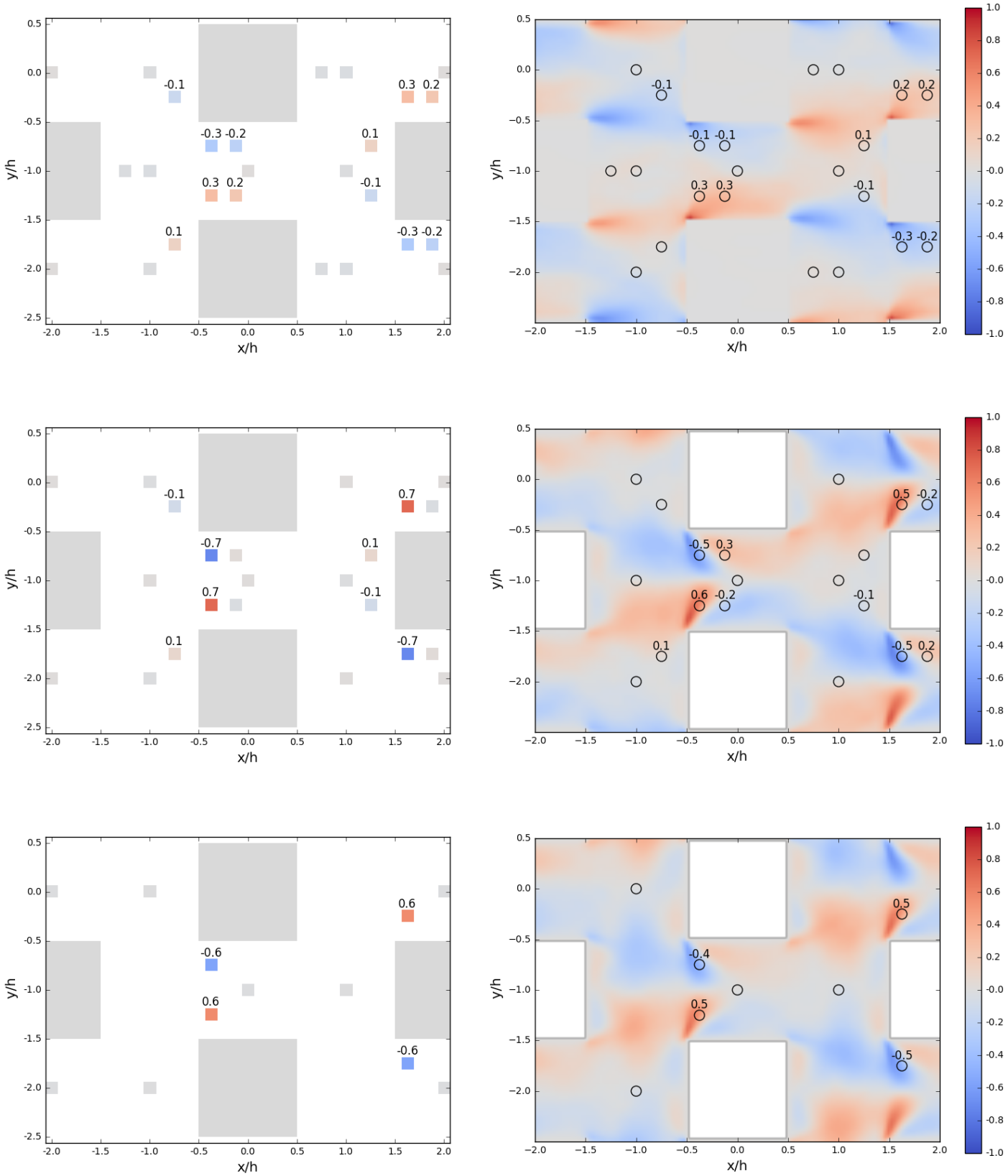

Figure 11: Maps of **Covariance of streamwise and spanwise velocity** $< uv > /u_*^2$ in wall-parallel planes inside the canopy at various heights : $z = h$ (top), $z = h/2$ (middle), $z = h/4$ (bottom), obtained with LDA data (left) and LES data (right). On the LES maps, the position of the LDA points have been reported with black circles. On both maps, numerical values of Covariance of streamwise and spanwise velocity $< uv > /u_*^2$ obtained at the positions of LDA points have been reported. The same colormap is used.

4 Spectral Analysis

The power spectra density on LES and LDA data were computed using a regular Welch FFT algorithm with block averaging (the block size was to 10 turn-over times). In order to use the FFT on LDA data, a resampling of the signal was performed at 2000 Hz with a linear interpolation scheme.

4.1 Scaling of the power spectral density and comparison between LDA and LES

The power spectral density on the streamwise velocity component of the LES and LDA data is shown on figure 12, at point P2 for the 3 heights inside the canopy. The PSD is normalized using the friction velocity u_*. On the left side graphs, spectra are in inner scaling; this scaling seems quite appropriate since there is now a collapse between the two datasets over one decade ($10^0 \leq \tilde{f} \leq 10^1$), located in the inertial subrange. This collapse is however very reduced at $z/h = 4$ where the LES spectra hardly show any inertial subrange and only tangentially approach the LDA spectra. At all heights, clear differences are noticeable at low frequencies $\tilde{f} \leq 10^0$ and at high frequencies $\tilde{f} \geq 10^1$; in both cases, the LES PSD is lower than the LDA one.

In the high frequency domain, the differences may be attributed to the cut-off frequency induced by the size of the mesh $\Delta = h/32$:

$$f_{LES,max} = \frac{u_*}{h/16}$$

In inner scaling this reads $\tilde{f}_{LES,max} = 16$. It is reported on figure 12 with a dashed line and indeed there is a good match with the frequency at which the LES start to fall-off from the LDA spectra. On the right-hand side graphs, the spectra are in outer-scaling, non-dimensionnalized using the bulk velocity $U_b = 2.6$ m/s and the height of the computational domain. As expected the LDA and LES spectra now collapse well in the low-frequency domain, with still a minimum frequency under which the LES seem to underestimate the spectral content of the flow. This difference may be attributed to the limited size of the LES computational box $[L_x, L_y, L_z] = [16h, 12h, 8h]$. Indeed, we can compute a cut-off frequency using the bulk velocity and the streamwise extent of the computational box:

$$f_{LES,min} = \frac{U_{bulk}}{L_x}$$

In outer scaling, this reads $\tilde{f}_{LES,min} = 0.5$. It is reported on figure 12 with a dashed line and indeed there is a good match with the frequency at which the LES start to fall-off from the LDA spectra.

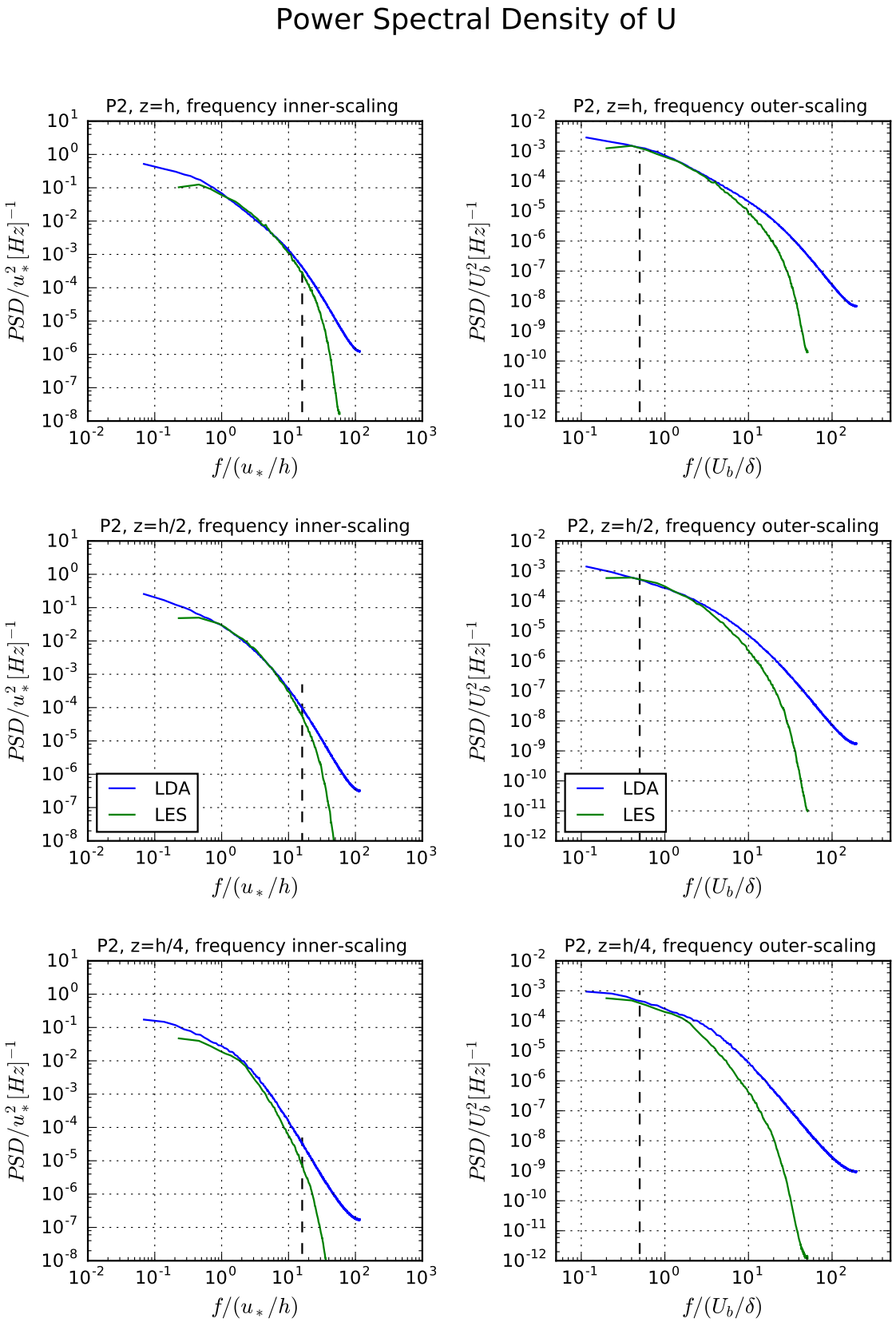

Figure 12: Power Spectral Density of U at P2 LES (green) and LDA (blue) data, at $z = h$ (top), $z = h/2$ (middle), $z = h/4$ (bottom), with inner scaling (left) and outer scaling (right) ; dashed line indicate the minimum and maximum frequency of the LES due to the size of the computational box and to the size of the mesh.

In figure 13, the same spectra are shown but in the pre-multiplied form. Here a clear trend with the wall normal distance is visible. The magnitude of the peak of energy increases with the wall normal distance on both dataset. It is of interest to see that the inner-scaling produces a better collapse of the energy decay, while the outer-scaling gives a better collapse of the peak of maximum energy. Inside the canopy, the origin of the energy may thus come from the flow outside the canopy, in the roughness or inertial sublayer. It is also important to see that the LES seems to resolve quite well both the peak of energy and the energy decay except below $z = h/2$ where the LES energy in the spectra is systematically lower.

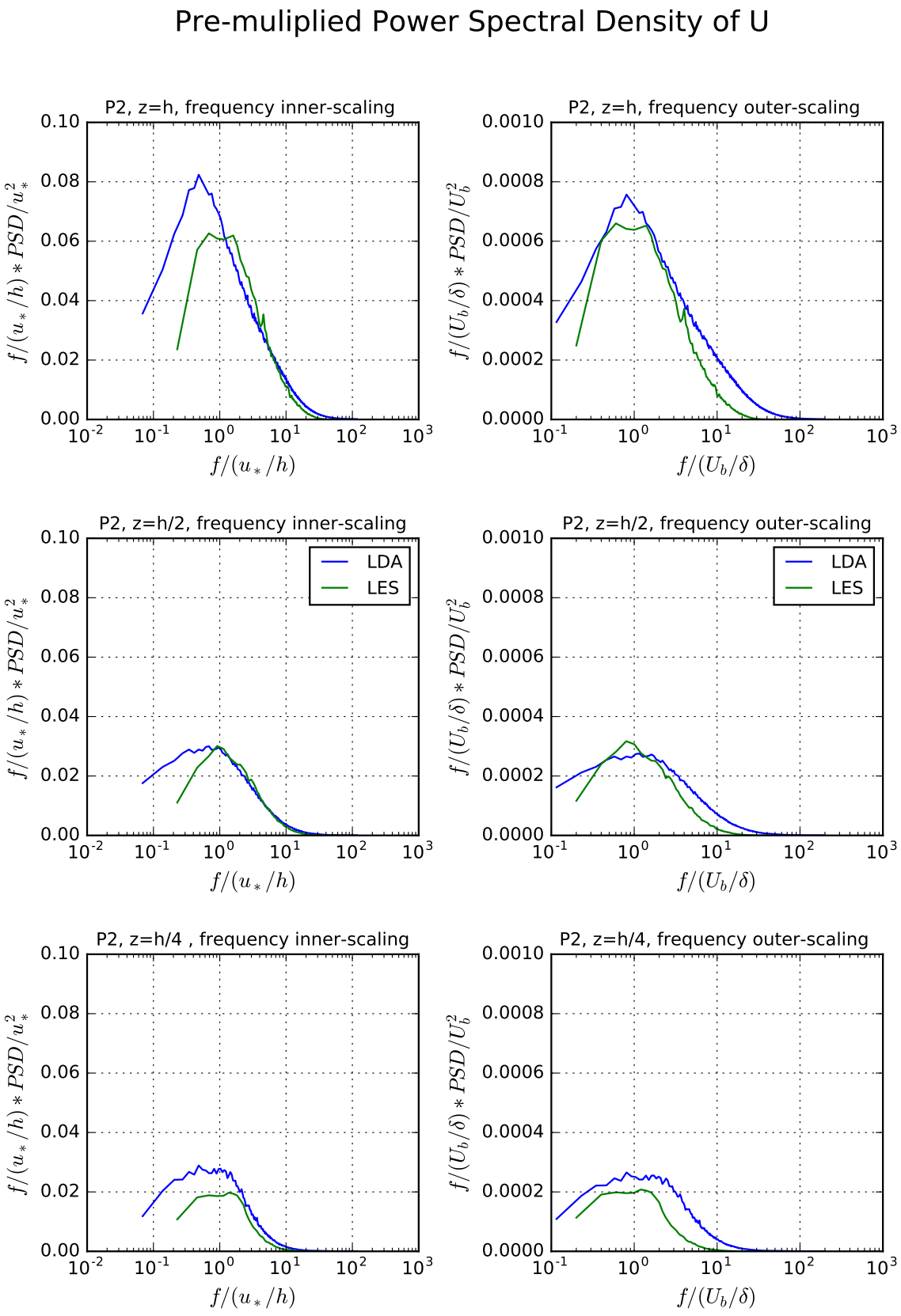

Figure 13: Pre-multiplied power Spectral Density of LES (green) and LDA (blue) data, at z=h (top), z=h/2 (middle), z=h/4 (bottom), with inner scaling (left) and outer scaling (right)

4.2 Evolution of the spectra with wall-normal distance

The power spectra density of the streamwise velocity obtained from the LDA data is shown in figure 14 and in the pre-multiplied form in figure 15 for each point at the different heights inside the canopy: $z = h/4$, $z = h/2$, $z = h$, in inner-scaling. The pre-multiplied spectra in outer scaling is also shown in figure 17. We added on each figure the power spectra measured above the canopy interface, in the roughness sublayer at $z = 1.25h$, $z = 1.45h$, and also at $z = 5h$, at point E. Due to the limitations discussed in section 4.1 about the lower and upper cutt-off frequency observed on the spectra obtained by LES, only spectra obtained by LDA are presented.
In the pre-multiplied form, the power spectra is found to be the highest in the roughness sublayer at $z = 1.25h$ and $z = 1.45h$, followed by the the inertial region ($z = 5h$), and finally by the canopy where the power spectra decreases with decreasing wall normal-distance, down to $z = h/2$.
In the vicinity of the wall ($z = h/2$ and $h/4$), the power spectra are almost identical.

Overall, at all points, the frequency at which the peak of pre-multiplied power spectra is observed is found to decrease with increasing wall normal distance, with energy containing eddies getting larger and/or slower. At $z = h/4$ and $h/2$, it is located at $\tilde{f} = 1$ in inner scaling ; for $z \geq h$ it is located at lower frequencies i.e. $0.1 \leq \tilde{f} \leq 1$.
The spectra at the canopy interface and in the roughness sublayer $z = h$, $1.25h$, $1.45h$ show a very good collapse in the inertial subrange, for $1 \leq \tilde{f} \leq 10$, with a logarithmic region of slope close to $-5/3$. In the inertial region $z = 5h$, the power spectra also display a logarithmic region, of slope close to $-5/3$. Close to the wall at $z = h/2$ and $z = h/4$, there is not such logarithmic region with a constant slope.
The pre-multiplied power spectra for the spanwise velocity component in inner scaling is shown in figure 16. The influence of the wall-normal distance, is less noticeable of v than on u component, and there is less difference of energy between the region above and the region within the canopy. Above the canopy and at the canopy interface, the power spectra on V is less energetic than on U, and the position of the main peak of energy is located at slightly higher frequencies, closer to $\tilde{f} = 1$ in inner scaling. Inside the canopy, the difference between the U and V component is less noticeable, probably because the flow is more three-dimensional in this region.

4.3 Comparison of the spectra within wall-parallel planes

The evolution of the power spectra of the streamwise velocity within wall-parallel planes inside the canopy is analyzed using the same figures 14, 15 and 17.
At the canopy interface ($z = h$), the maximum of energy is obtained at point P2 and C, followed by points B, A and P3, and finally by the downstream recirculation region of the cube at point P1 where the energy is the lowest, and where the peak is located at a frequency noticeably higher than other points.
At mid-height of the canopy, there is more energy in a streamwise alley in between two cubes (**C**, P3, B) than in the upstream (A, P2) and downstream region (P1) of a cube.
Close to the wall ($z = h/4$), we only have data at points P2, P3, and B. The maximum of energy is obtained at point B, followed by P3 and then by P2.
Interestingly, the pre-multiplied power spectra for the spanwise velocity component is found to be very energetic inside the canopy at point B, in possible connection with a vortex shedding or a flapping of the by-pass motion of the main flow between the right side and the left side of the cube. The region upstream of the cube at point P1 is also found to be quite energetic at $z = h/2$.

The power spectra of the spanwise component also show a broadening of the peak of energy at the canopy interface $z = h$. At points B, P1 and A a secondary peak seems to emerge: a first peak is at about $\tilde{f} \approx 1$ while the second one is centered at a higher frequency $\tilde{f} \approx 4$. This second peak may be associated to a vortex shedding or to flapping of the flow next to the cube ; the Strouhal number linked to a vortex shedding would then be about 4 in inner scaling.

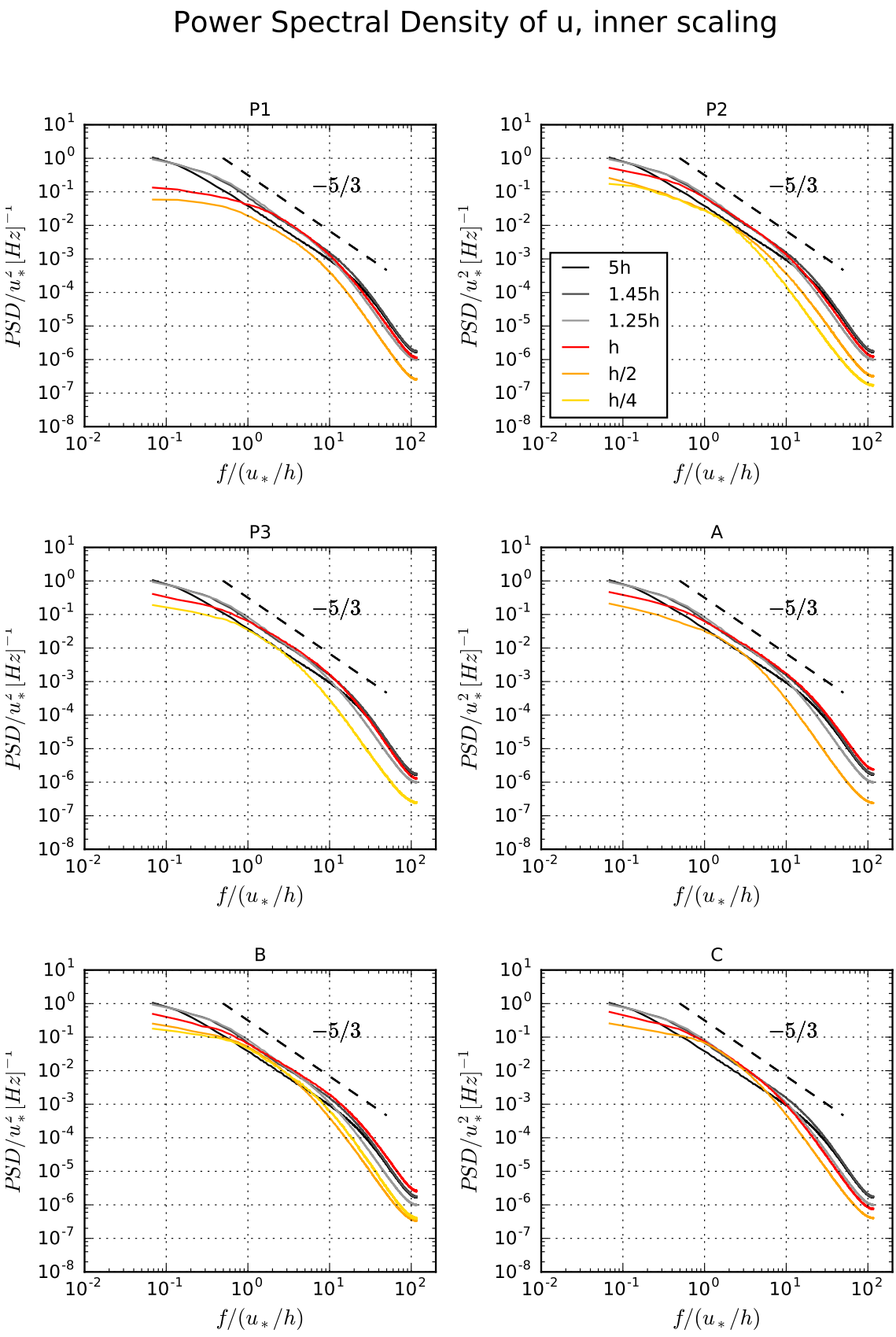

Figure 14: Power Spectral Density LDA data, at all measurement point and at all height, for **streamwise component**, in inner scaling

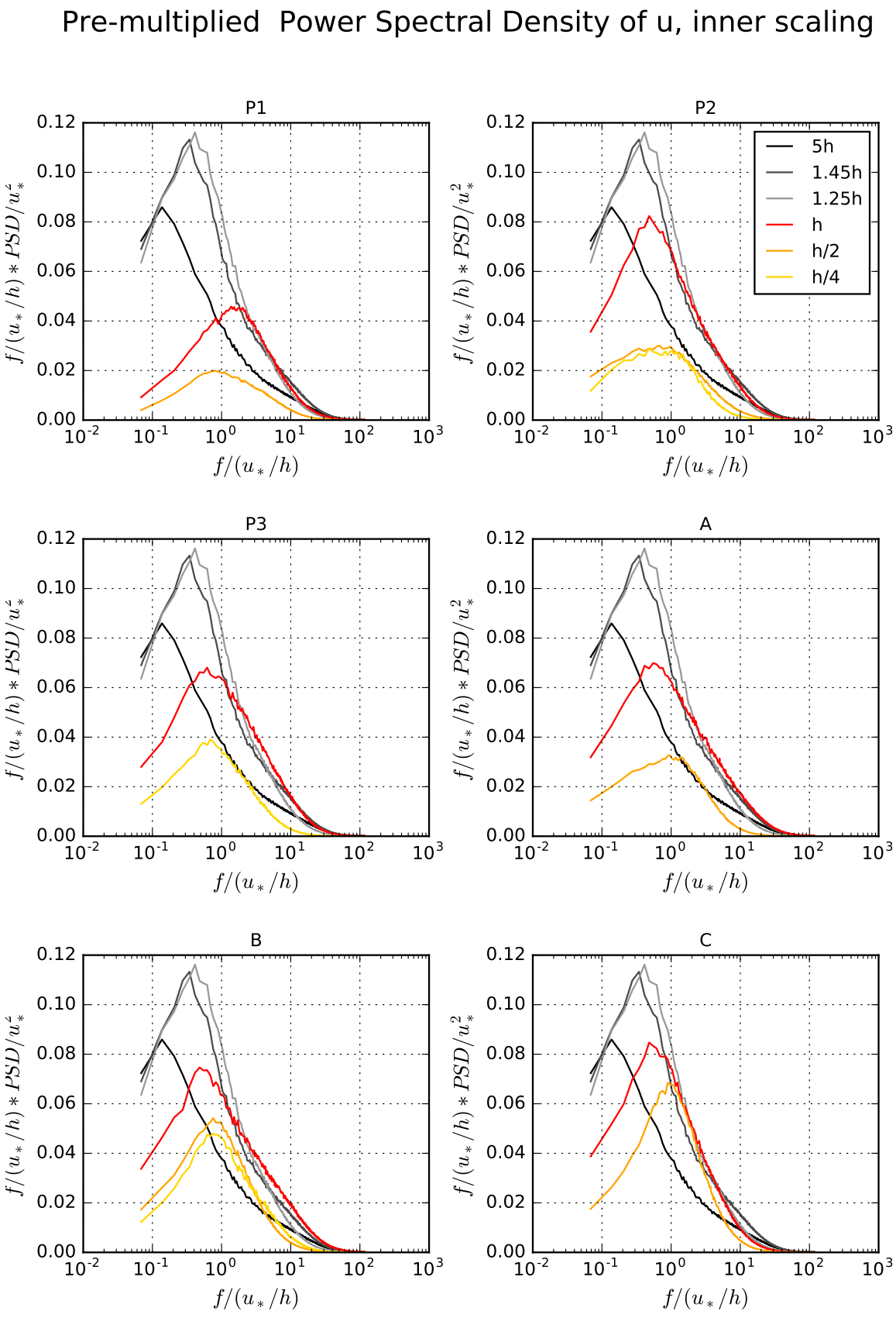

Figure 15: Pre-multiplied power Spectral Density LDA data, at all measurement points and at all heights, for the **streamwise component**, in inner scaling

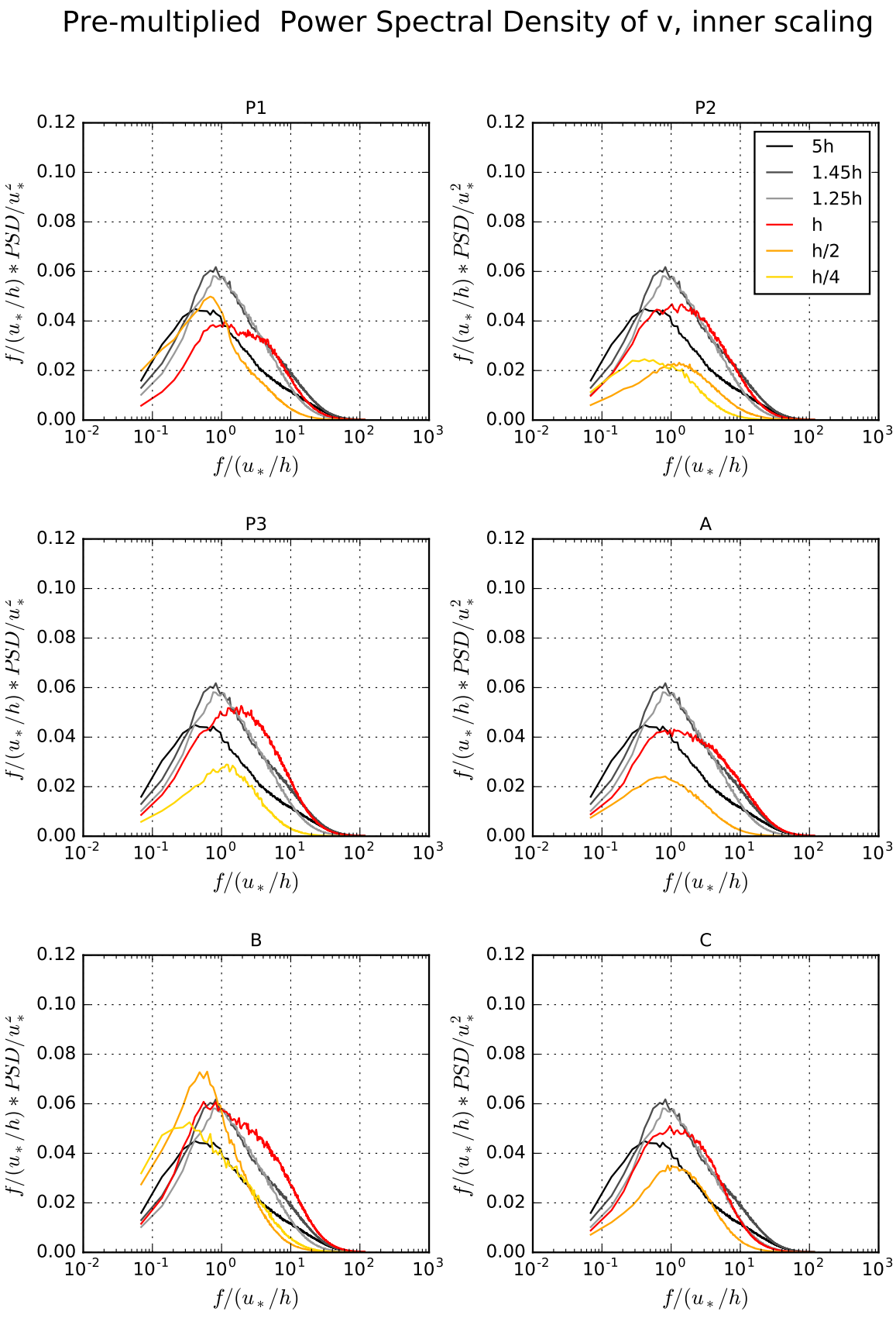

Figure 16: Pre-multiplied power Spectral Density LDA data, at all measurement points and at all heights, for the **spanwise component**, in inner scaling

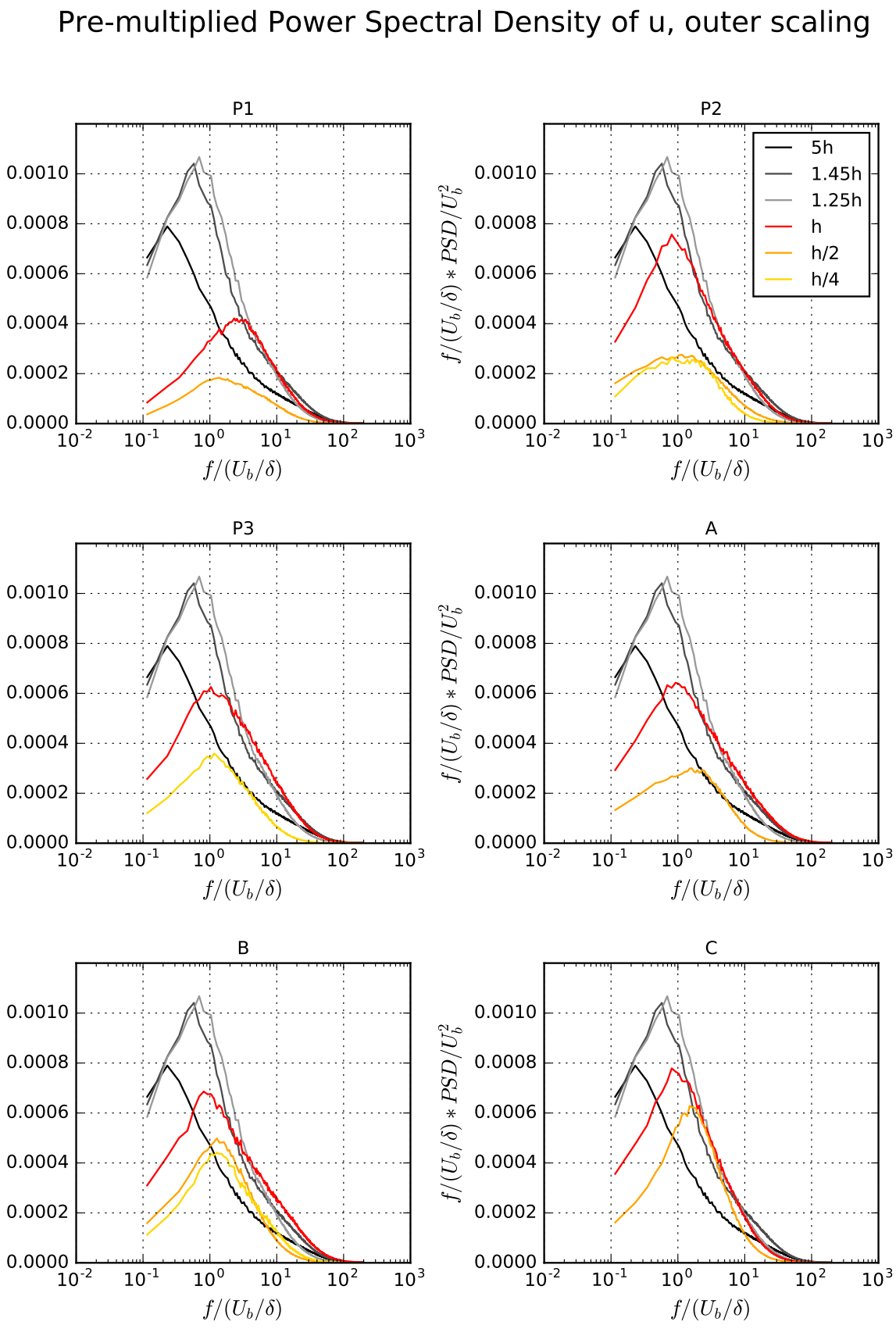

Figure 17: Pre-multiplied power Spectral Density LDA data, at all measurement points and at all heights, for the **streamwise component** in outer scaling

5 Conclusion

The flow inside an idealized urban canopy consisting of an staggered array of cubes with a 25% density, immersed into an atmospheric surface layer with a Reynolds number of $Re_\delta = \delta^+ = 32300$ has been investigated by means of Laser Doppler Anemometry and compared with a LES dataset of parameters similar to the DNS of [5]. The Reynolds number based on the cube height in the LDA and LES data are $h^+ = 1420$ and $h^+ = 500$ respectively. The wall-normal mean velocity profile and Reynolds stresses of both the LDA and LES data show a good agreement with available data in the literature, although some differences are observed on the standard deviation of the spanwise component. Maps of the flow in wall-parallel planes inside the canopy extracted from the LES data are analyzed and allow a better understanding of the organization of the flow inside the canopy. The mean streamwise velocity show a strong spatial variations in wall-parallel plane for $z \leq h/2$, with recirculation regions on the sides and in the downstream region of the cube, and a strong acceleration in the streamwise alley between cubes. At the canopy interface $z = h$, both the streamise and the spanwise component are found to more spatially homogeneous. For $z \leq h/2$, high values of σ_u, σ_v and $< uv >$ are consistently found on the sides of the cube at point B. The comparison of the temporal spectra between the LDA and the LES show a good collapse in the inertial range using an inner scaling, but discrepancies are observed at low and high frequencies. The differences are well explained with a minimum and a maximum cut-off frequency of the LES data linked to the limited size of the computationnal box $L_x = 16h$ and to the mesh grid size $\Delta = h/32$, respectively. A detailed spectral analysis is then carried out using the LDA data. To our knwowledge, this is the first time such results are shown on the evolution of the power spectral density inside the canopy. On the streamwise velocity component, the power spectral density in the inertial layer $z = 5h$, in the roughness sublayer $z = 1.45h$, $1.25h$ and at the canopy interface $z = h$ show a logarithmic region of slope close to $-5/3$. No such region is found for the spectra at $z = h/2$ and $z = h/4$. The maximum of energy on the streamwise velocity component is found in the roughness sublayer and then the energy decreases with decreasing wall-normal distance. At the canopy interface, the maximum of energy is obtained in the upstream region of the cube at $P2$ and at the corner of the cube at point C. The point in the downstream of the cube (P1) has the lowest energy and the peak is slighlty shifted to higher frequencies. At $z = h/2$, the highest energy is found at B and C probably linked to the vortex shedding activity in this region. The power spectral density of the spanwise component is also analyzed. It is found that the energy on the spanwise component is lower than on the streamwise component, but the energy variation is not monotonic anymore with wall normal distance. At points B, the peak of energy is higher inside the canopy than in the roughness sublayer, and a maximum is observed at $z = h/2$. An interesting phenomenon is also observed with a broadening of the energy peaks which may evoke the emergence of a secondary peak, especially at points $P1$, B, and A.

Acknowledgments

The authors wish to thank the financial support of the French National Research Agency through the research grant URBANTURB ANR-14-CE22-0012-01, as well as the technical support from Dantec Dynamics (Christian Tanguy and Jean-Jacques Lasserre) who provided the 2-Components Flow Explorer Laser Doppler System as well as technical guidance for the measurements.

References

[1] Karin Blackman and Laurent Perret. Non-linear interactions in a boundary layer developing over an array of cubes using stochastic estimation. *Physics of Fluids*, 28(9):095108, September 2016.

[2] Ian P. Castro, Hong Cheng, and Ryan Reynolds. Turbulence Over Urban-type Roughness: Deductions from Wind-tunnel Measurements. *Boundary-Layer Meteorology*, 118(1):109–131, January 2006.

[3] Hong Cheng and Ian P. Castro. Near wall flow over urban-like roughness. *Boundary-Layer Meteorology*, 104(2):229–259, 2002.

[4] O. Coceal, A. Dobre, T. G. Thomas, and S. E. Belcher. Structure of turbulent flow over regular arrays of cubical roughness. *Journal of Fluid Mechanics*, 589, October 2007.

[5] O. Coceal, T. G. Thomas, I. P. Castro, and S. E. Belcher. Mean Flow and Turbulence Statistics Over Groups of Urban-like Cubical Obstacles. *Boundary-Layer Meteorology*, 121(3):491–519, November 2006.

[6] C.S.B. Grimmond and T. R. Oke. Aerodynamics properties of urban area derived from analysis of surface form. *Journal of Applied Meteorology*, 1999.

[7] R.W. Macdonald, S. Carter, and P.R. Slawson. Measurements of Mean Velocity and Turbulence Statistics in Simple Obstacle Arrays at 1:200 Scale. Thermal Fluid Report 2000-1, University of Waterloo, Department of Mechanical Engineering, 2000.

[8] R. Martinuzzi and C. Tropea. The flow around surface-mounted, prismatic obstacles placed in a fully developed channel flow (data bank contribution). *Journal of Fluids Engineering*, 115(1):85–92, 1993.

[9] E.R. Meinders and K. Hanjalic. Vortex structure and heat transfer in turbulent flow over a wall-mounted matrix of cubes. *International Journal of Heat and Fluid Flow*, 20:255–267, 1999.

[10] T. R. Oke. Street Design and Urban Canopy Layer Climate. *Energy and Buildings*, pages 103–113, 1988.

[11] Laurent Perret, Thibaud Piquet, Jeremy Basley, and Romain Mathis. Effects of plan area densities of cubical roughness elements on turbulent boundary layers. In *Congrès Français de Mécanique*, 2017.

[12] Cedric Rivet. *Etude en soufflerie atmosphérique des interactions entre canopée urbaine et basse atmosphère par PIV stéréoscopique*. PhD thesis, Ecole Centrale de Nantes, 2014.

[13] J. Smagorinsky. General Circulation Experiments with the Primitive Equations. *Monthly Weather Review*, 91(63):99–164, 1963.

[14] J. Sousa. Turbulent flow around a surface-mounted obstacle using 2d-3c DPIV. *Experiments in Fluids*, 33(6):854–862, December 2002.